Surface Architectures Built around Perylenediimide Stacks

Charbonnaz, Pierre; Zhao, Yingjie; Turdean, Raluca; Lascano, Santiago; Sakai, Naomi; Matile, Stefan

How to cite

CHARBONNAZ, Pierre et al. Surface Architectures Built around Perylenediimide Stacks. In: Chemistry, 2014, vol. 20, n° 51, p. 17143–17151. doi: 10.1002/chem.201404423

This publication URL: https://archive-ouverte.unige.ch/unige:43005
Publication DOI: 10.1002/chem.201404423

Surface Architectures Built Around Perylenediimide Stacks

Pierre Charbonnaz, Yingjie Zhao, Raluca Turdean, Santiago Lascano, Naomi Sakai and Stefan Matile*[a]

[a] P. Charbonnaz, Dr. Y. Zhao, Dr. R. Turdean, S. Lascano, Dr. N. Sakai, Prof. S. Matile

Department of Organic Chemistry

University of Geneva, Geneva (Switzerland)

Fax: (+41) 22-379-3215

E-mail: stefan.matile@unige.ch

Homepage: www.unige.ch/sciences/chiorg/matile

Supporting information for this article is available on the WWW under http://www.chemeurj.org/ or from the author.

Abstract: Simple stacks of perylenediimides (PDIs) grown directly on solid surfaces are an intriguing starting point for the construction of multicomponent architectures because their intrinsic activity is already very high. Their ability to efficiently generate photocurrent originates from the strong absorption of visible light and the efficient transport of both electrons and holes after their generation with light. The objective of this study was to explore whether or not the excellent performance of these remarkably simple single-channel photosystems could be further improved in more sophisticated multicomponent architectures. We report that the directional construction of strings of anions or cations along the PDI stacks does not improve significantly their activity,

that is, the intrinsic activity of PDI stacks is too high to yield ion-gated photosystems. The directional construction of electron- and hole-transporting stacks of naphthalenediimides (NDIs) and oligothiophenes along the central PDI stack did not improve photocurrent generation under standard conditions either. However, the activity of double-channel photosystems increased with increasing thickness, whereas increasing charge recombination with single-channel PDI stacks resulted in decreasing activity with increasing length. Most efficient long-distance charge transport was found with double-channel photosystems composed of PDIs and NDIs. This suggested that over long distances, PDI stacks transport holes better than electrons, at least under the present conditions. Triple-channel photosystems built around PDI stacks with oligothiophenes and triphenylamines were less active, presumably because hole mobility in the added channels was inferior to that in the original PDI stacks, and thus promoted charge recombination.

Introduction

Perylenediimides (PDIs) are large aromatic molecules with strong absorption in the visible range.[1-6] The large, planar perylene core accounts for the formation of π-stacked aggregates in solution and in the solid state. PDIs are recognized n-type organic semiconductors, and their aggregates have high charge mobility perpendicular to the aromatic plane of the molecule. Due to these properties, PDIs have been extensively used in electro- and photoactive supramolecular systems, such as bioinspired dyads, one-dimensional aggregates, liquid crystals, and in organic field effect transistors, light-emitting diodes and organic solar cells. In the context of synthetic photosystems, supramolecular n/p-heterojunctions (SHJs) with co-axially aligned molecular-level conductive channels and related multicomponent architectures have been envisioned to maximize photogeneration of holes and electrons at the n/p-interface.[6,7] Due to their structural and optoelectronic properties, PDIs have been used to build SHJs in solution or as nanostructures

in the solid state using classical combinations of non-covalent interactions such as hydrogen bonding and *π*-stacking.[5,6]

Recently, self-organizing surface-initiated polymerization (SOSIP) has been introduced for the directional growth of stacks with naphthalenediimides (NDIs),[8] oligothiophenes[9] and PDIs[1-6] on indium tin oxide (ITO) surfaces.[10,11] The architectures obtained with PDIs showed the features of face-to-face *π*-stacking, and better *π*-stacking correlated with higher photoactivity.[11] Testifying for excellent light absorption and charge conductivity, photosystems made with PDIs gave already high photocurrents in single-channel architectures built by SOSIP.[11] Later on, SOSIP with templated stack exchange (TSE) has been introduced as a unique synthetic method to construct oriented and ordered multichannel architectures on ITO.[12] Functional multicomponent architectures with NDIs and oligothiophenes as central stacks with one or two co-axial stacks of fullerenes, squaraines, NDIs, PDIs, oligothiophenes, phthalocyanines and porphyrins have been prepared.[10,13,14] More recently, we reported ion-gated photosystems composed of central NDI stacks and lateral strings of ionized groups.[15]

In this report, we focus on multicomponent photosystems built by SOSIP-TSE around central PDI stacks. The outstanding properties of single PDI stacks are shown to hinder sensitivity toward ion gating and activation by charge separation in lateral triads in triple-channel photosystems but to enable charge transport over very long distances in double-channel SHJ photosystems, thus generating the highest photocurrents reported so far in comparable systems. Contrary to most reports in the literature, long-distance charge transport in SHJ photosystems is best with PDI stacks that function as hole transporters.

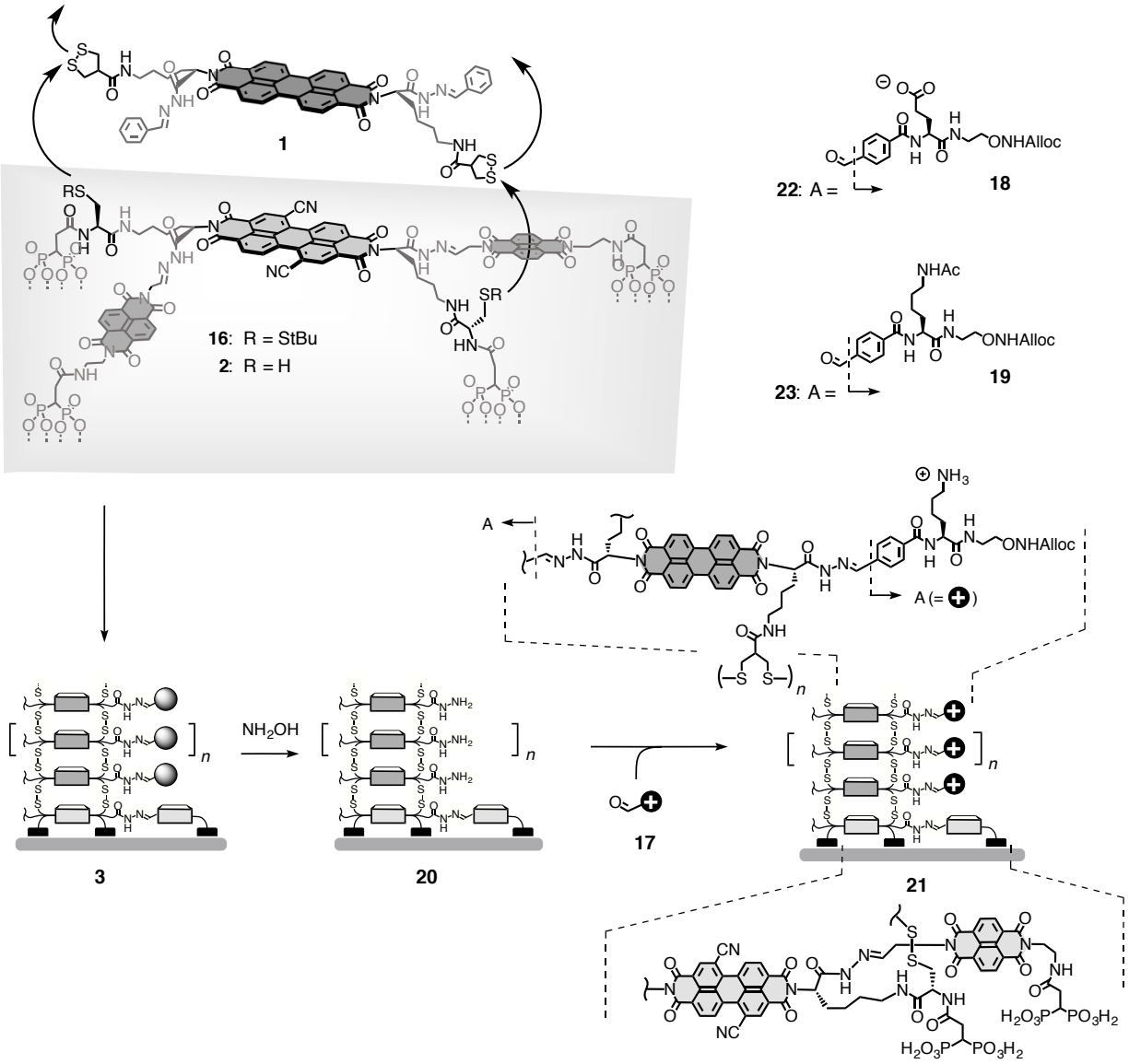

Figure 1. Propagator 1 and initiator 2 for SOSIP with PDIs on ITO, schematic structure of the resulting photosystem 3, and TSE with 17 to install strings of positive charges along the PDI stack in photosystem 21. TSE with 18 and 19 gives the corresponding anionic and neutral photosystems 22 and 23, respectively.

Results and Discussion

Propagator **1** and initiator **2** were designed to give PDI SOSIP architecture **3** with handles for further elaboration (Figure 1). Both contain central PDI chromophores installed in a peptide-like hydrogen-bonding network that works together with π-π stacking for the self-organization of the

system. The main chain of propagator **1** continues with strained cyclic disulfides from asparagusic acid for SOSIP by ring-opening disulfide-exchange polymerization,[16,17] the side chains with benzaldehyde hydrazones[17] to template for post-SOSIP TSE. The main chain of initiator **2** continues with thiolates to initiate ring-opening disulfide-exchange polymerization. The side chains of initiator **2** continue with NDI templates to reserve free space for post-SOSIP TSE. Both chains of initiator **2** finish with diphosphonates to bind to the ITO surface. The frontier molecular orbitals (FMOs) of the unsubstituted PDI in propagator **1** and the PDI in initiator **2** with two cyano substituents[1-3] in the core favor the injection of electrons and hinder the injection of holes into the ITO electrode.

All components used in this study were prepared by multistep synthesis from commercially available starting materials. Detailed procedures can be found in the Supporting Online Information. To prepare propagator **1**, perylenedianhydride **4** was reacted with Z-protected lysine **5** (Scheme 1). In the resulting PDI **6**, the two carboxylic acids were transformed into Boc-protected hydrazides. Then the Z-group in **7** was removed, and the liberated amines were reacted with activated asparagusic acid **8**. Removal of the Boc protecting groups in **9** and hydrazone formation with benzaldehyde gave propagator **1**.

The two cyano groups in the PDI core of initiator **2** had to be introduced at the beginning of the synthesis. Dibromination of perylenedianhydride **4** was achieved following reported procedures.[1-3] Reaction of the core-substituted product **10** with Z-lysine **5** followed by nucleophilic substitution in the core gave dicyano PDI **11**. As with the propagator, the free acids in PDI **11** were transformed into Boc-protected hydrazides. After removal of the Z-protecting groups in **12**, the liberated amines were reacted with Fmoc- and *tert*-butyl protected cysteine, the Fmoc was removed, and the liberated amines were reacted with acid **13**. Removal of Boc and Bn protecting groups in PDI **14** and hydrazone formation with the previously reported NDI aldehyde **15** then gave PDI **16** (Figure 1).

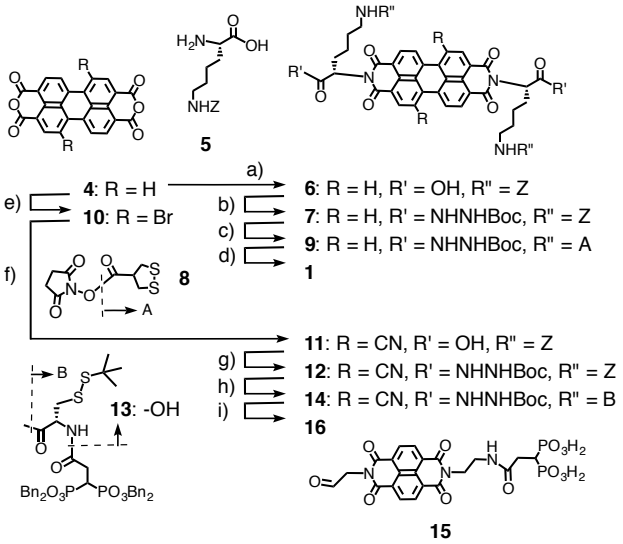

Scheme 1. a) Imidazole, 100 °C, 50 min; b) Boc-$NHNH_2$, HBTU, TEA, DMF, rt, 1 h, 73% (2 steps); c) 1. H_2, Pd/C, AcOH, MeOH, 1 h, rt, quant; 2. **8**, TEA, DMF, rt, 1 h, 67%; d) 1. TFA, thioanisole, DCM, rt, 1 h; 2. Benzaldehyde, rt, 15 min, 90% (2 steps); e) ref [2b]; f) 1. **5**, AcOH, NMP, 75 °C, 2 h, 87%; 2. dppf, $Zn(CN)_2$, $Pd_2(dpa)_3$, 1,4-dioxane, reflux, 12 h, 53%; g) Boc-$NHNH_2$, EDCI, DCM, 0 °C, 2 h, 91%; h) 1. H_2, Pd/C, AcOH, MeOH, 4 h, rt, quant; 2. Fmoc-Cys(S-*t*-Bu)-OH, HBTU, collidine, HOBt, DMF, rt, 1 h, 52%; 3. TBAF, DMF, rt; 4. **13**, HBTU, collidine, DMF, rt, 11% (2 steps); i) 1. TMSBr, DCM, rt, 3 h; 2. MeOH, rt, 4 h; 3. **15**, DMSO, AcOH, rt, 24 h.

To prepare for SOSIP,[10,11] ITO electrodes were dipped for 48 hours into a 0.5 mM solution of PDI **16** in DMSO. The surface coverage estimated from cyclic voltammetry and ferricyanide reduction inhibition were consistent with the presence of a compact monolayer. Deprotection of the thiols directly on the surface by incubation for 1 hour in 15 mM aqueous DTT gave initiator **2** (Figure 1).

Propagator **1** and Hünig's base as a catalyst were added next to initiate SOSIP. The choice of solvents for SOSIP is critical and needs careful optimization. In the deaerated mixture $CHCl_3$/MeOH 5:2, SOSIP occurred at a concentration $c_{SOSIP} \approx 13$ mM in the presence of initiator **2**, whereas polymerization did not occur on ITO surfaces without initiator **2** under the same

conditions (Figure 2a). The directional growth of PDI stacks **3** by SOSIP was followed by the increase of the absorption maximum of PDIs at 543 nm.

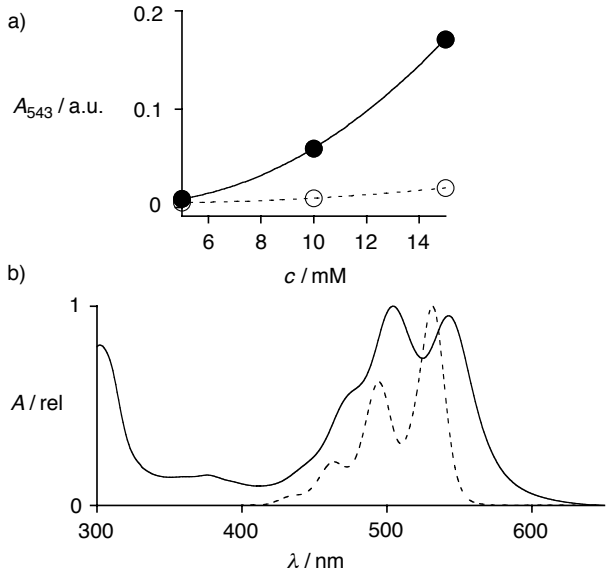

Figure 2. a) Absorption of ITO electrodes with (●) and without (○) initiator **2** after incubation with propagator **1** at varied concentrations *c* and 100 mM Hünig's base in $CHCl_3$/MeOH 5:2. b) Absorption spectra of photosystem **3** (solid) and propagator **1** in CH_2Cl_2/MeOH 3:1 (dotted).

The absorption spectrum of the resulting photosystem **3** is shown on Figure 2b (solid) together with absorption spectrum of propagator **1** in solution (Figure 2b, dotted). In solution, the main absorption band displayed a well-resolved vibronic structure with S_0-S_1 transition at 531 nm and S_0-S_2 at 494 nm. The absorption spectrum of photosystem **3** displayed broader, less resolved bands. The absorption maximum corresponding to the S_0-S_1 transition was hypsochromically shifted by 26 nm (970 cm^{-1}), to 505 nm, and a red-shifted band appeared at 543 nm. These features are characteristic for face-to-face π-stacked PDIs in H-aggregates with the optical transition into the higher energy exciton being allowed. The bathochromic band arises from rotational displacement between neighboring chromophores that allows optical transition into the lower energy exciton.[1,2,11] Film thickness (*d*), that is the formal length of the PDI stacks, was estimated from their absorption. Assuming a repeat distance of 3.5 Å in an ideal π-stack

perpendicular to the surface, an absorbance at 543 nm of A_{543} = 0.1 a.u. was approximated to correspond to $d \approx 44$ nm.

With derivatizable single PDI stacks on ITO in hand, ion-gated photosystems were explored first. For this purpose, stack exchangers **17**-**19** were synthesized following reported procedures (Figure 1).[15] They all contain an aldehyde for TSE and a protected hydroxylamine for eventual further extension by oxime formation. Stack exchanger **17** further contains an ammonium cation, stack exchanger **18** contains a carboxylate anion, and stack exchanger **19** serves as an uncharged control. For TSE,[12-15] photosystem **3** was dipped for 24 hours into 1 M aqueous NH_2OH to remove benzaldehyde templates. The obtained photosystem **20** was immediately immersed into 20 mM solution of stack exchanger **17** in DMSO/AcOH 9:1 to fill the large holes drilled along the PDI stacks by reversible hydrazone formation. Immediate completion of TSE with freshly prepared photosystems **20** is in general very important to achieve high TSE yield.

The obtained photosystem **21** with strings of cations along the PDI stack was equilibrated in buffer at pH 7.5. Both removal of the benzaldehydes and formation of hydrazones were monitored by changes in absorption at 305 nm. The photosystem **22** with strings of anionic glutamate along the PDI stack and the neutral control system **23** were prepared similarly from photosystem **20** and aldehydes **18** and **19**, respectively. Yields of TSE reactions were high (~80%) with thin photosystems (A_{543} < 0.1 or d < 44 nm) but decreased with thicker ones to still acceptable 66% (A_{543} < 1.3 or d < 570 nm).

The importance of ion gating for photocurrent generation with single PDI stacks was evaluated under routine conditions. The photosystems were used as working electrodes in the presence of triethanolamine (TEOA) as a mobile hole acceptor in solution, a Pt wire as a counter electrode, and Ag/AgCl as a reference electrode. When measured at pH 7.7, photocurrent generation by photosystems **21**-**23** increased linearly with increasing thickness of the photosystems up to a thickness of $d \approx 90$ nm, independent of the presence or absence of charges (Figure 3a). In thicker films at $A_{543} > 1$, i.e. $d > 400$ nm, photocurrents decreased with increasing thickness (Figure 3b).

This absence of long-distance charge transport was found for the original uncharged photosystem **3** and for the anionic photosystem **22**. Moreover, photocurrents generated at pH 7.7 were recorded as a function of the temperature, and the data fitted to the Arrhenius equation ($k = A \exp(-E_a/RT)$).[15,18] The obtained values for activation energy E_a did not change much in the presence of co-axial strings of cations and anions (i.e., E_a (**3**) = 0.18 eV > E_a (**22**) = 0.17 eV > E_a (**21**) = 0.13 eV). The found differences presumably originated from differences in thickness rather than from ion gating ((i.e., A_{543} (**3**) = 0.07 > A_{543} (**22**) = 0.05 > A_{543} (**21**) = 0.04) and remained significantly below the ones obtained with NDI photosystems (0.40 > E_a > 0.19 eV).[15] These findings suggested that, contrary to the less active single NDI stacks, the more active single PDI stacks do not respond to ion gating.

The validity of this interpretation was further supported by the pH profiles of PDI photosystems. With increasing pH, photosystems **21**-**23** generated gradually more photocurrent (Figure 3c). This increase originates from the gradual deprotonation of the TEOA hole acceptor in solution and has nothing to do with the properties of the photosystems. Most importantly, the anionic photosystem **22** did not show a bell-shaped behavior with a maximum around pH 7.5. This behavior of PDI stacks was contrary to that of NDI stacks, demonstrating that partial deprotonation of the co-axial strings of anions did not help to isolate, stabilize and transport holes by hole/proton antiport.[15]

Taken together, the absence of bell-shaped pH profiles, the constantly low activation energies and the decreasing rather than increasing activity in thicker films demonstrated that single PDI stacks do not form ion-gated photosystem. Unlike the underperforming NDI stacks,[15] the intrinsic properties of single PDI stacks are already too good to further improve with ion gating. From a technical point of view, the reliable trends obtained for the dependence of photocurrent generation on pH and thickness nicely illustrate that SOSIP-TSE with PDI stacks is highly reproducible as long as conditions are carefully optimized and precisely followed. The same reliability of the

SOSIP-TSE method can be seen in the plots for double-channel photosystems described in the following.

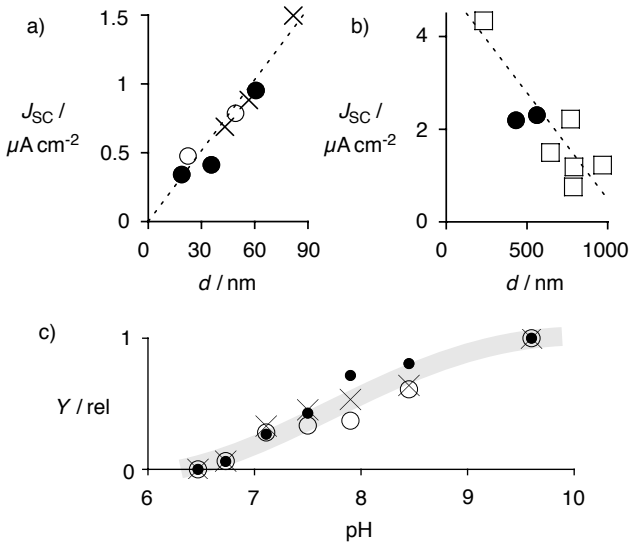

Figure 3. Photocurrent generated by photosystems **21** (○), **22** (●), **23** (X), and **3** (□) irradiated with a solar simulator (P = 83 mW cm^{-2}; 50 mM TEOA; 0.2 M $Na_mH_nPO_4$ buffer; pH = 7.7 at 0 V vs Ag/AgCl). Film thickness d was approximated from PDI absorption assuming that A_{543} = 0.1 a.u. corresponds to $d \approx 44$ nm (a, b). pH dependence of the activity of photosystems **21** (○), **22** (●) and **23** (X) irradiated with a solar simulator (P = 83 mW cm^{-2}; 50 mM TEOA; 0.2 M $Na_mH_nPO_4$ buffer; pH = 6.5−9.6 at 0 V vs Ag/AgCl), $Y = [J - J(\text{pH } 6.5)] / [J(\text{pH } 9.6) - J(\text{pH } 6.5)]$ (c). Dotted (a, b) and grey lines (c) are added as visual guides.

Double-channel SHJ architectures built around central PDI stacks were explored next. The previously reported terthiophene stack exchanger **24**[14][19] was selected to build hole-transporting channels along the central PDI stack (Figure 4). The aldehyde acceptor at one terminus was needed for TSE, the methoxy donor at the other side to increase the energy of the HOMO to -5.41 eV and thus maximize hole accepting and transporting abilities (Figure 4). The methyl groups along the scaffold were of interest to further raise the HOMO energy by hyperconjugation and to weakly deplanarize the terthiophene in solution and thus maximize solubility. Planarization

of the weakly twisted chromophore in a π-stack should be unproblematic.[19] Comparison with the FMO levels of the PDI stack suggested that hole injection into the terthiophene channel after excitation of the PDI should be very favorable. The same would be true for electron injection into the PDI stack after excitation of the terthiophene.

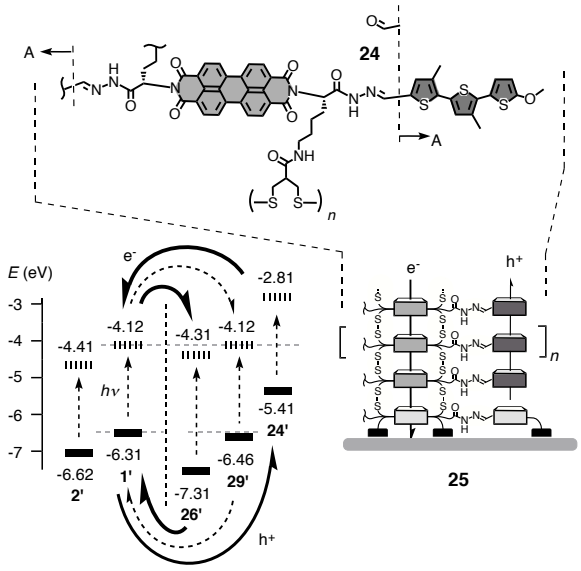

Figure 4. Schematic structure of double-channel photosystem **25** with HOMO (bold) and LUMO (dashed) energy levels against vacuum of PDIs **1'** and **2'**, terthiophenes **24'** (hydrazone derivative) and NDIs **26'** and **29'**. They refer to suitable derivatives of the respective chromophores and were taken from the literature or determined by cyclic voltammetry for pertinent derivatives of the shown structures and are reported relative to -5.1 eV for Fc^+/Fc.

The double-channel photosystem **25** was readily accessible by TSE (Figure 4). The hydrazide-rich photosystem **20** was prepared from photosystem **3** as described above and immediately immersed in 15 mM terthiophene **24** in DMSO/AcOH 9:1. Replacement of the benzaldehydes in photosystem **3** with terthiophenes in **25** was correctly reflected by the appearance of a nicely separated absorption band at 385 nm (Figure 5a). Quantification of the ratio between PDI and lateral chromophores using their respective extinction coefficients from their absorption spectra

in solution was not accurate because of the characteristic hypochromism of the π-stacked PDI. Therefore, stack exchange yields were estimated from absorption spectra in solution obtained after dissolving the various architectures using mercaptoethanol. Unsurprisingly, TSE with the small and well soluble aldehyde **24** proceeded in quantitative yield even with very thick films (A_{543} > 1 or d >400 nm). The circular dichroism (CD) spectra of single PDI stacks **3** showed strong bisignate Cotton effects, whereas those of double-channel architectures **25**, were consistent with preferable exciton coupling between the PDI and the terthiophene stacks at preserved *M*-helical twist (Figure S5).[20]

In short stacks with A_{543} < 0.6 or d < 260 nm, double-channel photosystem **25** and single-channel photosystem **3** generated about the same amount of photocurrent, showing that the high activity of **3** was not improved by addition of the hole-transporting channel (Figure 6). With increasing thickness, the short-circuit current density generated by single-channel photosystem **3** saturated at J_{SC} = 8.0 μA cm^{-2} around $d \approx$ 260 nm, and decreased significantly with longer stacks (Figure 6, □, Table 1). The dependence of photocurrent generation on temperature revealed that decreasing photocurrents with increasing thickness coincide with an increase in activation energy from E_a = 177 meV up to E_a = 298 meV. The thickness dependence of the bimolecular charge recombination efficiencies η_{BR} was approximated from the dependence of photocurrent generation on the irradiation intensity as described.[21,12,14] Increasing efficiencies from η_{BR} = 30% up to η_{BR} = 70% confirmed that charge recombination accounts for the decreasing photocurrent generation by PDI stacks that are longer than $d \approx$ 260 nm. This meant that single PDI stacks, despite otherwise outstanding properties, were incapable to mediate charge transport over very long distances.

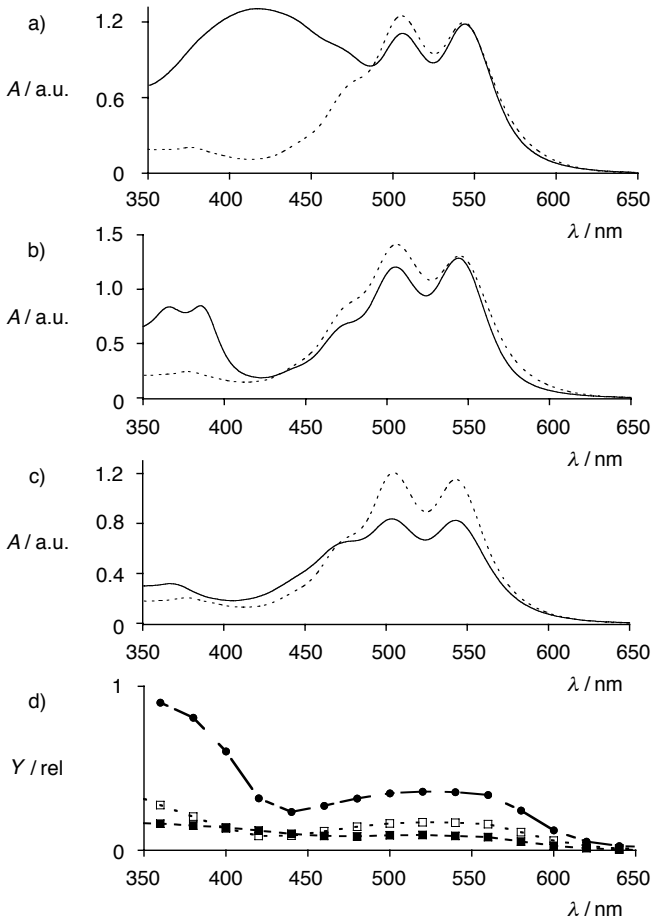

Figure 5. a) Absorption spectra during (**20**, dotted) and after (**25**, solid) TSE with **24**. b) Absorption spectra during (**20**, dotted) and after (**26**, solid) TSE with **27**. c) Absorption spectra during (**20**, dotted) and after (**30**, solid) TSE with **29**. d) Action spectra of photosystems **3** (□), **25** (■) and **26** (●). Y = IPCE/(1-T_{543}), IPCE = incident photon-to-current efficiency, T_{543} transmittance at 543 nm.

Compared to single-channel photosystem **3**, photocurrents generated by double-channel photosystem **25** saturated at clearly higher J_{SC} = 13.8 μA cm^{-2} and clearly longer distances of d ≈ 500 nm (Figure 6, ■, Table 1). Double-channel stacks of d ≈ 1 µm length still generated photocurrents of J_{SC} = 12.5 μA cm^{-2}. This quite remarkable long-distance charge transport was possible because contrary to single-channel photosystem **3**, activation energies and bimolecular

charge recombination efficiencies of double-channel photosystem **25** did not increase with thickness. Even at a length of $d \approx 1$ µm, excellent E_a = 177 meV and η_{BR} = 29% were found.

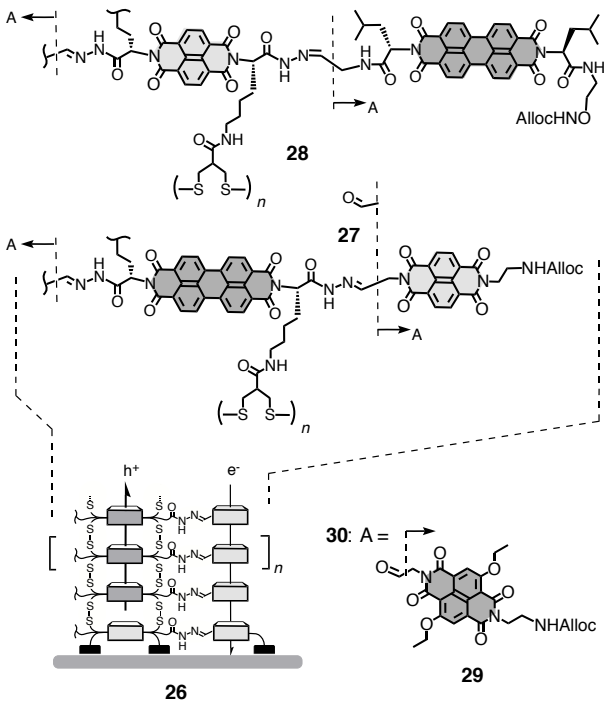

Figure 6. Dependence of the short-circuit current density J_{sc} on the thickness for photosystems **3** (□), **25** (■), **26** (●) and **30** (○) upon irradiation with a solar simulator (83 mW cm^{-2}; 50 mM TEOA, 0.1 M Na_2SO_4, 0 V vs Ag/AgCl). Film thickness *d* was approximated from PDI absorption assuming that A_{543} = 0.1 a.u. corresponds to $d \approx 44$ nm, pertinent values for bimolecular charge recombination efficiencies η_{BR} (from dependence of J_{sc} on irradiation intensity) and activation energy E_a (from dependence of J_{sc} on irradiation intensity) are indicated.

In double-channel photosystem **25**, PDI stacks are expected to transport electrons, whereas the co-axial terthiophene stack should transport holes. In double-channel photosystem **26** with co-axial NDI channels, the roles were reversed (Figure 7). The LUMO level of NDIs is with -4.31 eV clearly below that of PDIs at -4.12 eV (Figure 4). The central PDI stacks should thus transport the holes, whereas the co-axial NDI stacks should transport electrons. Aldehyde **27** was synthesized according to reported procedures[12] and covalently captured by photosystem **20**. The formation of photosystem **26** was correctly reflected by the appearance of the NDI absorption

maximum at 380 nm with preserved vibronic fine structure (Figure 5b). For photosystems **26**, the yields of TSE were, with 52-80%, acceptable but below the quantitative ones for photosystem **25**. This was consistent with the lower solubility of the planar NDIs in aprotic polar solvents.

Photocurrents generated by double-channel photosystem **26** with A_{543} < 0.6 were undistinguishable from those generated by single-channel photosystem **3** and double-channel photosystem **25**. With increasing thickness, photocurrents generated by double-channel photosystem **26** continuously increased up to J_{SC} = 22 μA cm^{-2} with formal stacks of 1 µm length (A_{543} = 2.4, Figure 6, ●, Table 1). This quite remarkable ability to transport charges over very long distances coincided with a thickness independence of the relatively high bimolecular charge recombination efficiency at η_{BR} = 39% and a comparably high, thickness dependent activation energy E_a = 239 meV. This result confirmed the crucial role of the second channel to prevent charge recombination in long stacks. Better photocurrent generation by double-channel photosystem **26** with electron-transporting NDI stacks compared to double-channel photosystem **25** with hole-transporting oligothiophene stacks suggested that PDI stacks preferably transport holes under these conditions. Although the ambipolar nature of PDIs is documented theoretically and experimentally,[6] this result was interesting because PDIs are usually perceived and used as n-semiconductors.[1-7]

The superb activity of PDI-NDI photosystem **26** was also interesting with regard to the previously reported NDI-PDI photosystem **28** (Figure 7).[14] This reversed architecture **28** gave also very high activity, although clearly below that of **26**. However, with NDI-PDI photosystem **28**, it was not possible to assess the importance of the NDI channel because single-channel NDI photosystems are poorly active, and all activity found with double-channel NDI-PDI photosystem **28** could originate from the PDI channel added by TSE. With single-channel PDI photosystems **3** in hand, the functional relevance of the NDI channel could be clarified. Namely, the additional NDI channels are irrelevant for photocurrent generation with short stacks up to ~250 nm but

essential for the generation of the most important photocurrents by long-distance charge transport in double-channel stacks as long as 1 μm.

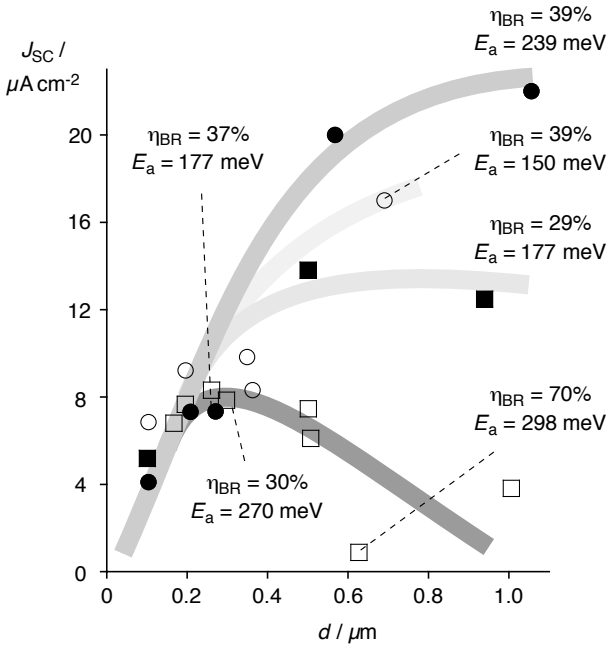

Figure 7. Schematic structure of double-channel photosystem **26** and **30** in comparison with the previously reported reversed architecture in **28**.

Table 1. Summary of Photosystems with Central PDI Stacks.

Entry	PS [a]	Architecture [b]	ΔE / eV [c]	TSE / % [d]	d / nm [e]	J_{SC} / μA cm^{-2} [f]	η_{BR} / % [g]	E_a / meV [h]	Figures [i]
1	**3**	Single channel	-	-	31	0.7	31	180	1, 2, 6
2				-	165	6.7	30	240	
3				-	625	0.9	70	298	
4	**26**	Double channel (NDI)	-0.19 / -1.00	52	270	7.3	37	177	4, 6, 7,
5				71	1055	22.0	39	239	5b, 5d

6	**30**	Double channel (NDI)	0.00 / 0.15	-	72	350	9.8	34	230	4, 6, 7,
7					60	690	17.0	39	150	5c
8	**25**	Double channel (OT)	+1.31 / +0.90		100	100	5.2	31	169	4, 6,
9					100	940	12.5	29	177	5a, 5d
10	**34**	Double channel (OT)	+0.92 / +0.53		100	115	4.9	44	270	8
11					81	555	0.9	54	296	
12	**31**	Triple channel	+1.57 / +0.76		100	40	2.5			8
13					95	265	0.9			
14	**22**	Ion gated (-)	-		80	19	0.4		130	1, 3
15	**21**	Ion gated (+)	-		88	22	0.5		170	1, 3

[a] Photosystems. [b] General characteristics, compare text (OT = oligothiophene). [c] Difference of the energy of the LUMO (left) and HOMO (right) compared to that of PDI. [d] Yield of templated stack exchange. [e] Film thickness *d* was approximated from PDI absorption assuming that A_{543} = 0.1 a.u. corresponds to $d \approx 44$ nm. [f] Bimolecular charge recombination efficiency, estimated from the dependence of photocurrents on irradiation intensity. [g] Activation energy, estimated from the dependence of photocurrents on temperature. [i] Reference to figures with structures, details, and original data.

Interestingly, η_{BR} and E_a were better with the less active photosystem **25** with hole-transporting oligothiophenes. This suggested that the high activity of double-channel photosystem **26** with electron-transporting NDIs originates from favorable separation of electrons and holes. The action spectra of the two photosystems were in support of this interpretation. Action spectra report incident-photon-to-current efficiencies (IPCEs) at individual wavelength. The action spectrum of double-channel photosystem **26** with electron-transporting NDIs showed strong maxima around

380 nm and 540 nm, confirming that both NDI and PDI contribute significantly to photocurrent generation (Figure 5d, ●). In particular, clearly higher IPCE observed for NDIs compared to PDIs despite lower absorbance indicated that photoinduced hole transfer from NDI to PDI (ΔE = -1.00 eV) is more efficient than electron transfer from PDI to NDI (ΔE = -0.19 eV, Figure 4, Table 1). In sharp contrast, the action spectrum of double-channel photosystem **25** with hole-transporting oligothiophenes was weaker than the one measured for single-channel photosystem **3** (Figure 5d, ■ vs □). These results were in agreement with the interpretation that improved charge separation mainly accounts for long-distance charge transport with photosystem **26** with hole-transporting PDI stacks, whereas minimized charge recombination accounts for that of photosystem **25** with electron-transporting PDI stacks.

Aldehyde **29** was synthesized to build double-channel photosystem **30** (Figure 7). This architecture was interesting because the FMO levels of the yellow NDIs with two alkoxy groups in the core are nearly identical with the ones of the PDIs in the central stacks (Figure 7).[8] Their respective position suggested that the PDIs could still act as very weak electron donors and stronger hole acceptors, i.e., function as hole transporters (Figure 4). The installation of the co-axial NDI stacks was detectable by the appearance of a shoulder at 476 nm (Figure 5c, solid). The obtained stack-exchange yields were with 60-80% in the range of the ones obtained with photosystems **26**. Contrary to single-channel photosystem **3**, double-channel photosystem **30** was capable of long-distance charge transport (Figure 6, ○, Table 1). This finding demonstrated that the NDI channel contributes to long-distance charge transport by keeping the recombination of the charges separated into the two channels reasonably low and by minimizing activation energies. As expected from the similar FMO levels and in clear contrast to photosystem **26**, charge separation did not appear very favorable and did thus not account for long-distance charge transport (low IPCE in action spectrum, slightly stronger than with **3** and with a shoulder for the yellow NDI, Figure S9). Despite these slightly different origins, efficient long-distance transport by double-channel photosystem **30** supported the conclusion from double-channel photosystem

26 that PDIs serve better as hole transporters than as electron transporters as in the less performing double-channel photosystem **25**.

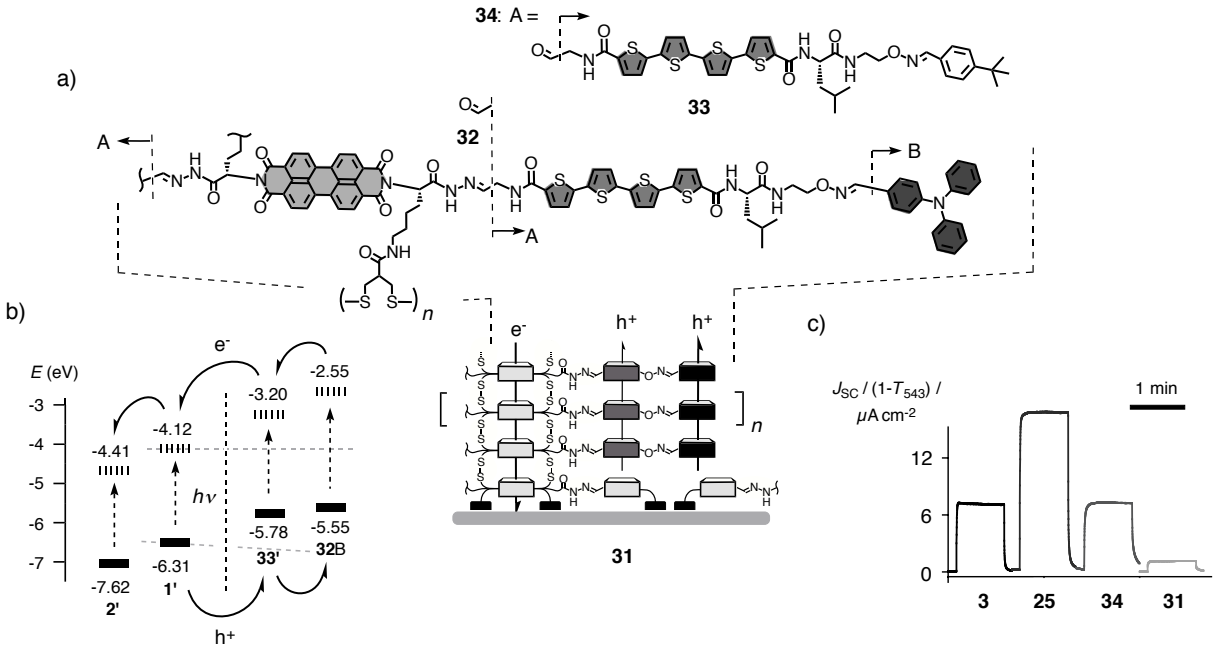

Figure 8. a) Schematic structure of triple-channel photosystem **31** and control double-channel photosystem **33**. b) HOMO (bold) and LUMO (dashed) energy levels against vacuum of PDIs **1'** and **2'**, quaterthiophenes **33'** and TPA **32**B (suitable derivatives of the respective chromophores), reported relative to -5.1 eV for Fc+/Fc. c) Photocurrent generated by photosystems **3**, **25**, **34** and **31** of similar thickness (left to right), irradiated with a solar simulator (83 mW cm^{-2}; 50 mM TEOA, 0.1 M Na_2SO_4, 0 V vs Ag/AgCl), normalized against transmittance *T* at 543 nm.

The functional significance of double-channel photosystems called for the construction of triple-channel architectures **31** from central PDI stacks (Figure 8a). Together with PDIs, the added quaterthiophenes[13] and triphenylamines[14,7a] form a triad that could drive holes and electrons toward triphenylamines and PDIs, respectively (Figure 8b). With hole- and electron-transporting pathways further apart, charge recombination could further decrease. Dyad **32** was synthesized in a few steps from previously reported intermediates. Monitored by absorption spectroscopy, TSE with PDI stacks **20** occurred in excellent 95-100%. However, photocurrents generated by

triple-channel system **31** were very weak (J_{SC} = 2.5 μA cm^{-2} at A_{543} = 0.09) and decreased significantly with increasing thickness (Table 1). To better understand this poor performance, control molecule **33**[13] containing the inactive *t*-butylphenyl instead of the active TPA was installed in photosystem **20** in 81-100% yield to afford double-channel photosystem **34** (Figure 8a). The activity of PDI-quaterthiophene photosystem **34** was intermediate between the less active triple-channel photosystem **31** and the more active PDI-terthiophene photosystem **25** (Figure 8c). The better performance of **25** compared to **34** was consistent with the higher HOMO level of methoxy-terthiophenes in the former (-5.41 eV, Figure 4) compared to quaterthiophenes in the latter (-5.78 eV, Figure 8b). Almost the same could be said for the TPA hole acceptor in triple channel photosystem **31** (-5.55 eV, Figure 8b, Table 1). The poor activity with horizontal triads is in striking contrast with the high activity with vertical triads in SOSIP-TSE photosystems, that is triple-gradient double-channel photosystems.

Conclusions

The specific objective of this report was to learn whether or not the superb intrinsic properties of single PDI stacks could be further improved in multicomponent surface architectures. We show that ion-gated and triple-channel architectures fail to do so. However, in double-channel architectures, so-called supramolecular heterojunctions, the highly performing central PDI stacks are the key to achieve charge transport over very long distances. Double-channel architectures reliably show thickness dependent increase of photocurrent up to $d \approx 1$ µm. This is the longest charge transport observed so far, and the magnitude of the generated photocurrent is unprecedented in comparable systems. Interestingly, electron-transporting channels formed by NDI stacks along the central PDI stacks give better activities than co-axial hole-transporting channels formed by oligothiophenes. This suggests that, contrary to most reports in the literature, PDI stacks function better as hole- than as electron-transporting channel in double-channel architectures. The origin of this high activity with hole-transporting PDI stacks is attributed to

favorable photoinduced charge separation, whereas minimized charge recombination and activation energies account presumably for long-distance charge transport with electron-transporting PDI stacks. A summary overview of all prepared photosystems is presented in Table 1.

Unprecedented photocurrent generation with charge transport over the longest ever reported distances in SOSIP-TSE architectures demonstrates the potential of photosystems built around central PDI stacks. Their comprehensive analysis in multicomponent architectures of appreciable sophistication further confirms the power of synthetic methods that operate with orthogonal dynamic covalent bonds[17] (i.e., self-organizing surface-initiated polymerization, templated stack exchange) to elaborate on multichannel architectures with molecule-level precision and without interference from thermodynamically preferred but inactive mixed donor-acceptor systems. Alternative synthetic methods that would provide access to similar insights do not exist today.

Acknowledgements

We thank A. Fin, H. Shaw and D.-H. Tran for contributions to synthesis, D. Jeannerat, M. Pupier and S. Grass for NMR measurements, the Science Mass Spectroscopy (SMS) platform for mass spectrometry service, and the University of Geneva, the European Research Council (ERC Advanced Investigator), the National Centre of Competence in Research (NCCR) in Chemical Biology, the NCCR Molecular Systems Engineering, and the Swiss NSF for financial support.

[1] F. Würthner, *Chem. Commun.* **2004**, *40*, 1564-1579.

[2] a) X. Zhang, D. Görl, V. Stepanenko, F. Würthner, *Angew. Chem.* **2014**, *126*, 1294-1298; *Angew. Chem. Int. Ed.* **2014**, *53*, 1270-1274; b) Z. Chen, U. Baumeister, C. Tschierske, F. Würthner, *Chem. Eur. J.* **2007**, *13*, 450-465.

[3] M. R. Wasielewski, *Acc. Chem. Res.* **2009**, *42*, 1910-1921.

[4] a) D. Baumstark, H.-A. Wagenknecht, *Angew. Chem.* **2008**, *120*, 2652-2654; *Angew. Chem. Int. Ed.* **2008**, *47*, 2612-2614; b) K. Sugiyasu, S.-i. Kawano, N. Fujita, S. Shinkai, *Chem. Mater.* **2008**, *20*, 2863-2865; c) R. Marty, R. Nigon, D. Leite, H. Frauenrath, *J. Am. Chem. Soc.* **2014**, *136*, 3919-3927; d) A. D. Shaller, W. Wang, H. Gan, A. D. Q. Li, *Angew. Chem.* **2008**, *120*, 7819-7823; *Angew. Chem. Int. Ed.* **2008**, *47*, 7705-7709; e) M. Probst, D. Wenger, S. M. Biner, R. Häner, *Org. Biomol. Chem.* **2012**, *10*, 755-759.

[5] a) F. Würthner, Z. Chen, F. J. M. Hoeben, P. Osswald, C.-C. You, P. Jonkheijm, J. van Herrikhuyzen, A. P. H. J. Schenning, P. P. A. M. van der Schoot, E. W. Meijer, E. H. A. Beckers, S. C. J. Meskers, R. A. J. Janssen, *J. Am. Chem. Soc.* **2004**, *126*, 10611-10618; b) S. Foster, C. E. Finlayson, P. E. Keivanidis, Y.-S. Huang, I. Hwang, R. H. Friend, M. B. J. Otten, L.-P. Lu, E. Schwartz, R. J. M. Nolte, A. E. Rowan, *Macromolecules* **2009**, *42*, 2023-2030; c) W.-S. Li, A. Saeki, Y. Yamamoto, T. Fukushima, S. Seki, N. Ishii, K. Kato, M. Takata, T. Aida, *Chem. Asian J.* **2010**, *5*, 1566-1572; d) L. F. Dössel, V. Kamm, I. A. Howard, F. Laquai, W. Pisula, X. Feng, C. Li, M. Takase, T. Kudernac, S. De Feyter, K. Müllen, *J. Am. Chem. Soc.* **2012**, *134*, 5876-5886.

[6] a) T. B. Singh, S. Erten, S. Günes, C. Zafer, G. Turkmen, B. Kuban, Y. Teoman, N. S. Sariciftci, S. Icli, *Org. Electron.* **2006**, *7*, 480-489; b) J. Vura-Weis, M. A. Ratner, M. R. Wasielewski, *J. Am. Chem. Soc.* **2010**, *132*, 1738-1739.

[7] a) E. Busseron, Y. Ruff, E. Moulin, N. Giuseppone, *Nanoscale* **2013**, *5*, 7098-7140; b) T. Marangoni, D. Bonifazi, *Nanoscale* **2013**, *5*, 8837-8851; c) D. M. Bassani, L. Jonusauskaite, A. Lavie-Cambot, N. D. McClenaghan, J.-L. Pozzo, D. Ray, G. Vives, *Coord. Chem. Rev.* **2010**, *254*, 2429-2445; d) M. Morisue, S. Yamatsu, N. Haruta, Y. Kobuke, *Chem. Eur. J.* **2005**, *11*, 5563-5574; e) F. G. Brunetti, C. Romero-Nieto, J. López-Andarias, C. Atienza, J. L. López, D. M. Guldi, N. Martín, *Angew. Chem.* **2013**, *125*, 2236-2240; *Angew. Chem. Int. Ed.* **2013**, *52*, 2180-2184.

[8] S.-L. Suraru, F. Würthner, *Angew. Chem.* **2014**, *126*, 7558-7578; *Angew. Chem. Int. Ed.* **2014**, *53*, 7428-7448.

[9] A. Mishra, P. Bäuerle, *Angew. Chem.* **2012**, *124*, 2060-2109; *Angew. Chem. Int. Ed.* **2012**, *51*, 2020-2067.

[10] a) N. Sakai, M. Lista, O. Kel, S.-i. Sakurai, D. Emery, J. Mareda, E. Vauthey, S. Matile, *J. Am. Chem. Soc.* **2011**, *133*, 15224-15227; b) M. Lista, J. Areephong, N. Sakai, S. Matile, *J. Am. Chem. Soc.* **2011**, *133*, 15228-15231; c) E. Orentas, M. Lista, N.-T. Lin, N. Sakai, S. Matile, *Nat. Chem.* **2012**, *4*, 746-750.

[11] P. Charbonnaz, N. Sakai, S. Matile, *Chem. Sci.* **2012**, *3*, 1492-1496.

[12] N. Sakai, S. Matile, *J. Am. Chem. Soc.* **2011**, *133*, 18542-18545.

[13] A. Bolag, J. López-Andarias, S. Lascano, S. Soleimanpour, C. Atienza, N. Sakai, N. Martín, S. Matile, *Angew. Chem.* **2014**, *126*, 4990-4995; *Angew. Chem. Int. Ed.* **2014**, *53*, 4890-4895.

[14] G. Sforazzini, E. Orentas, A. Bolag, N. Sakai, S. Matile, *J. Am. Chem. Soc.* **2013**, *135*, 12082-12090.

[15] N. Sakai, P. Charbonnaz, S. Ward, S. Matile, *J. Am. Chem. Soc.* **2014**, *136*, 5575-5578.

[16] G. Gasparini, E.-K. Bang, G. Molinard, D. V. Tulumello, S. Ward, S. O. Kelley, A. Roux, N. Sakai, S. Matile, *J. Am. Chem. Soc.* **2014**, *136*, 6069-6074.

[17] A. Wilson, G. Gasparini, S. Matile, *Chem. Soc. Rev.* **2014**, *43*, 1948-1962.

[18] I. Riedel, J. Parisi, V. Dyakonov, L. Lutsen, D. Vanderzande, J. C. Hummelen, *Adv. Funct. Mater.* **2004**, *14*, 38-44.

[19] D. Alonso Doval, M. Dal Molin, S. Ward, A. Fin, N. Sakai, S. Matile, *Chem. Sci.* **2014**, *5*, 2819-2825.

[20] a) G. Pescitelli, L. Di Bari, N. Berova, *Chem. Soc. Rev.* **2014**, *43*, 5211-5233; b) P. Talukdar, G. Bollot, J. Mareda, N. Sakai, S. Matile, *Chem. Eur. J.* **2005**, *11*, 6525-6532.

[21] L. J. A. Koster, M. Kemerink, M. M. Wienk, K. Maturová, R. A. J. Janssen, *Adv. Mater.* **2011**, *23*, 1670-1674.